HSR-GEE: A 1-m GEE Automated Land Surface Temperature Downscaling System over CONUS

Mario Mhawej[1], Yaser Abunnasr[1]

[1] Department of Landscape Design and Ecosystem Management, Faculty of Agricultural and Food Sciences, American
University of Beirut, Bliss St., Beirut 2020-1100, Lebanon

Correspondence to: Yaser Abunnasr (ya20@aub.edu.lb)

Abstract. Downscaling remote sensing-based Land Surface Temperature (LST) datasets is of paramount importance for multiple research fields including urban heating, irrigation scheduling, volcanic monitoring, to name a few. Even with the constant development in technology, especially improvements in spatial, temporal and spectral resolutions of satellite sensors, global satellites are limited to a 60-m LST datasets at best. In this study, we use the massive computation power and large dataset directory found in the Google Earth Engine (GEE) platform to design a 1-m fully-automated, open-source and user-friendly LST downscaling system, named High Spatial Resolution-GEE or HSR-GEE. It has the ability to downscale Landsat-8 LST, combined with the National Agriculture Imagery Program (NAIP) images, into 1-m HSR LSTs over the CONUS and at Landsat-8 overpass time. Using only red, green, blue and near infrared bands, HSR-GEE implements multiple machine learning approaches, including, Robust Least Square (RLS), Random Forests (RF), and Support Vector Machine (SVM), along with comparison to two commonly-known and classical methods: the disaggregation procedure for radiometric surface temperature (DisTrad) and thermal sharpening (TsHARP). We validate HSR-GEE outputs against multiple airborne thermal images over the USA. We obtained a MAE of 1.92°C, 2.53°C, 1.33°C, 3.42°C and 3.4°C for the RLS, RF, SVM, DisTrad and TsHARP, respectively. With RF showing visually salt and pepper effect and SVM a Land Cover/Use form, the RLS appears to be most suited for 1-m LST downscaling. HSR-GEE is proposed as a high-potential system aiding researchers from different backgrounds to advance their research. HSR-GEE remains the only available 1-m GEE-based downscaling system that is able to derive the needed high resolution LST information in a matter of seconds and in five different approaches (i.e., RLS, RF, SVM, DisTrad and TsHARP). The research community is invited to implement this dynamic system over CONUS and enhance it if deemed necessary.

1 Introduction

Approaches aiming to increase the spatial resolution of a coarse image input based on better spatial resolution auxiliary datasets fall under downscaling or spatial sharpening techniques (Zakšek and Oštir, 2012; Gao et al., 2012; Essa et al., 2013; Jian and Wen, 2017; Wang et al., 2020). Land Surface Temperature (LST) is usually computed from satellite and airborne measurements and remains the most widely used variable at the fine and regional scales. Another important aspect of LST is

30   its ability to spatially represent, contrary to air temperature, the studied area. LST is also known for its inherited low spatial resolution, with the best raw spatial resolution of 60-m found in Landsat-7. Fine scale LST datasets are pivotal for multiple research disciplines, including urban heat fluxes and configuration (e.g., Bonafoni, 2016; Xue et al., 2020; Abunnasr et al., 2022), urban heat island (e.g., Stathopoulou and Cartalis, 2009; Dialesandro et al., 2019), wildfire and forest health (e.g., Mhawej et al., 2017; Cho et al., 2018; Maiti et al., 2018), water management and governance (e.g., Mhawej et al., 2020a;

35   Allam et al., 2020), and aridity and drought (e.g., Allaw et al., 2015; Faour et al., 2015; Faour et al., 2016).

LST downscaling approaches can be divided into the physical and the statistical methods. In the first type, a dual band method (e.g., Dozier, 1981; Giglio et al., 2003) and an emissivity-based approach (e.g., Liu and Pu, 2008; Zhan et al., 2013) are usually used. In the second, a statistical relationship between the coarse resolution LST and the improved spatial resolution auxiliary datasets is established. Among the most widely used auxiliary datasets, the Fraction of Vegetation Cover

40   (FVC), which is generated from the Normalized Difference Vegetation Index (NDVI), remains the most adequate (Agam et al., 2007).

Nonetheless, using only biophysical indices, such as NDVI and FVC, does not explain all variations in LST at the sub-pixel level, particularly over heterogeneous and complex landscapes (Gao et al., 2012). Even when successful, implementing these much-sophisticated statistical-based approaches (Hutengs and Vohland, 2016) along their transferability to other regions

45   other than the research study cases (Pan et al., 2018) pose major issues. To overcome these limitations, several automated algorithms were proposed in the last two decades, perhaps the most widely used are the disaggregation procedure for radiometric surface temperature (DisTrad) (Kustas et al., 2003), thermal sharpening (TsHARP) (Agam et al., 2007), and data mining sharpener (DMS) (Gao et al., 2012).

The applied approach in each of these previous models and systems may also differ. For instance, Kustas et al. (2003) with

50   their widely known DisTrad model used a least-square fit method with a Root Mean Square Error (RMSE) of 1.35°C when disaggregating 768-m pixel resolution to 192-m and a RMSE of 1.61°C between 1536-m and 192-m disaggregation. TsHARP, described in Agam et al. (2007), used almost identical least square fit method but where the independent variable is the FVC instead of the NDVI used in DisTrad. A cross-evaluation of the 60-m generated product to the original coarse resolution 960-m image showed a Mean Absolute Error (MAE) of 0.91°C. On the other hand, Zakšek and Oštir (2012) used

55   a Principal Component Analysis (PCA) to downscale ~5-km SEVIRI spatial resolution to 1-km spatial resolution with a RMSE of 2.5°C when inter-compared to MODIS LST level 2 product. In Bechtel et al. (2012), the Minimum Redundancy Maximal Relevance (MRMR) and the Forward selection approaches were used to downscale geostationary LST data 2000 times arriving at 100-m spatial resolution. The cross-evaluation to the original coarse resolution product showed a RMSE of 2.2°C. Machine learning Random Forest (RF) ensemble method is widely used lately for downscaling LST (e.g., Hutengs

60   and Vohland, 2016, Yang et al., 2017, Xu et al., 2021) with a RMSE ranging between 0.84 and 2.52°C. All these models and systems produce downscaled LST images that are suitable for studies that focus on coarse scale landscapes. On the other hand, when considering environmental planning at finer scales such as urban neighbourhoods or local site scale, obtaining

fine scale LST mapping is needed to identify features that contribute to local climate variations that impact larger phenomenon such as the Urban Heat Island or outdoor thermal comfort.

65 Our search of the literature has not identified any specific studies that address LST downscaling with very High Spatial Resolution (HSR) satellite images at a pixel size of around 1x1 meter. Furthermore, downscaling using easily available high-resolution images with the four visible bands (i.e., Red, Green, Blue, Near infrared (RGBN)) is non-existent in the surveyed literature. This has resulted in a very limited number of LST-based space borne research conducted at the district- and neighborhood-scales (Demuzere et al., 2014). Using only RGBN bands is particularly very attractive as it is commonly

70 available in many HSR free-to-access and commercial images. This presents an opportunity to increase downscaling applications to extremely fine resolutions without the use of hyper-spectral images or band widths that are only available at high cost.

In this context, this research proposes a dynamic, open-access, fully-automated and user-friendly RGBN-only LST downscaling approach, named HSR-GEE. It is based on Landsat-8 bands along 1-m HSR images and is hosted over the

75 Google Earth Engine (GEE) platform. The selected study area includes three regions in the Continental United States (CONUS) which are also used for validation using airborne thermal images. The following sections of the paper will describe the datasets used and the pre-processing techniques employed, introduce the HSR-GEE system and demonstrate its performance in each of the five approaches (i.e., Robust Least Square (RLS), RF, Support Vector Machine (SVM), DisTrad and TsHARP) embedded within HSR-GEE. It will be followed by a discussion of findings and main conclusions.

80 **2 Materials and Methods**

2.1 Data Background and Pre-processing

The study areas (Figure 1) correspond to three regions in the CONUS that include Hat Creek, California; Elkhorn, Nebraska; and Claryville, New York. We use high thermal infrared (TIR) images captured on December 15th, 2017 over the lower ElKhorn River and the adjacent urban area in Nebraska, USA (Hobza and Strauch, 2019). The final processed image is a 0.5

85 by 0.5 m grid of corrected surface temperatures, already computed by Hobza and Strauch (2019). The dataset encompasses a 16 Km reach of the river, from 0.64 Km upstream from USGS streamflow-gaging station number 06800500, Elkhorn River at Waterloo, Nebraska, to 2.9 Km downstream from USGS site number 06800800, Elkhorn River at Q St Bridge near Venice, Nebraska.

We also use high-resolution aerial LST images over the Hat Creek area in California, USA captured in the morning of

90 August 25th, 2018 (Curtis et al., 2018). The high-resolution airborne TIR surveys were conducted using a helicopter. The TIR images contain corrected 0.5-m surface temperatures in degrees Celsius and encompass a 64.6-km reach of Hat Creek that extends from 50 m upstream of the confluence with Lost Creek to 50 m downstream of the confluence with the Pit River.

In addition, we use TIR images captured between December 8th and 10th, 2019 over the river corridor encompassing two
95 U.S. Geological Survey Next Generation Water Observing Systems (NGWOS) stream gage locations near Claryville, NY,
USA. One site is the West Branch Neversink River at Claryville, NY (USGS station number 01434498) and the second is
Neversink River at Claryville, NY (USGS station number 01435000) (Briggs et al., 2020). The final unmanned aviation
system-based visible-light imagery is already calibrated 0.12 by 0.12 m grid of corrected surface temperatures.

Concerning the satellite-based inputs, HSR images were retrieved from the 1-m National Agriculture Imagery Program
100 (NAIP) with four different visible bands (RGBN). NAIP acquires images every three years since 2009 aerial imagery during
the agricultural growing seasons over the CONUS. Landsat-8 satellite is the second satellite-based dataset used in this
research and provides 30-m images of the earth surface across different wavelengths every 16 days since operational date on
February 11, 2013. Two 100-m resolution thermal band sensors are mounted on the satellite to assess the skin temperature of
the Earth or the LST. In this study, the 30-m USGS Landsat 8 Level 2, Collection 2, Tier 1 product is used. The atmospheric
105 correction used corresponds to the Land Surface Reflectance Code (LaSRC) algorithm. These datasets are accessible and
already   fully   processed   over   the   GEE   at   https://developers.google.com/earth-
engine/datasets/catalog/LANDSAT_LC08_C02_T1_L2.

Following the best practices for satellite-derived LST product validation described in Guillevic et al. (2018), we validate the
HSR-GEE outputs against the Hat Creek, ElKhorn and Claryville airborne thermal infrared images. To be able to do conduct
110 the validation, a normalization approach was applied as described in Pu and Bonafoni (2021) to retrieve the dTHR to
compensate for the different acquisition times (Table 1) and wavelengths between the TIR and Landsat 8 products. dTHR is
generated by subtracting the upscaled 2-time airborne LST over ElKhorn and Hat Creek and 8-time over Claryville from the
Landsat 8 LST products, to arrive at a spatial resolution of 1-m, followed by a spatial co-registration between the two
products from NAIP and TIR. dTHR layer, computed once for each date and over each region, was later added to the HSR-
115 GEE outputs. A comparison is made between these latter, where the dTHR for each date and region is now included, and the
1-m TIR LST images. Root Mean Square Error (RMSE) and Mean Absolute Error (MAE) can be then computed.

2.2 HSR-GEE System Development

The GEE platform, which the HSR-GEE system is based on, is a planetary-scale cloud system consisting of a multi-petabyte
analysis-ready datasets along an unparalleled computation service. It enables any interested party to effectively and promptly
120 address a variety of high-impact societal issues by monitoring and understanding local climatic events. By accessing its large
available datasets, GEE aims towards accelerating the sharing of knowledge and more adequate mitigation plans and
responses (Gorelick et al., 2017).

The following steps were automatically produced within the HSR-GEE model. First, we prepare the required input data,
namely Landsat 8 and NAIP. We apply a simple cloud masking approach to the Landsat 8 satellite images found over the
125 GEE platform based on cloud detection/quality assessment band (i.e., qa_pixel) to eliminate any pixel classified as cloud or
cloud shadow. This is followed by a bandpass adjustment process to calibrate NAIP RGBN and Landsat 8 cloud-free RGBN

bands as suggested in Claverie et al. (2018). The bandpass adjustment is based on a linear fit relationship between the red band from a NAIP image and the red band from the Landsat 8 image. The same applies to the other bands. This would generate the required slopes and intercepts to adjust each of the NAIP's bands to Landsat 8 bands' values. As a result, a new

130 NAIP image with updated RGBN values is created. We then compute Landsat 8 LST data by applying a scale (i.e., 0.00341802) along an offset (i.e., 149) to the cloud-free Landsat 8 thermal datasets previously generated and as indicated in the product manual. Furthermore, we aggregate Landsat 8 LST images with a cell factor of 30 to generate Very Low Spatial Resolution (VLSR) LST images with a spatial resolution of 900-m. This cell factor is particularly selected as being similar to the ratio between NAIP and Landsat 8 spatial resolutions (i.e., 1-m NAIP vs. 30-m Landsat 8 and 30-m Landsat 8 vs. 900-m

135 VLSR LST) and therefore enabling consistent transferability across different resolutions.

Second, we apply five different statistical based approaches (i.e., RLS, DisTrad, TsHARP, RF and SVM) to the inputs, including Landsat-8 RGBN bands, Landsat-8 LST, VLSR LST and adjusted NAIP RGBN bands. The best spatial resolution in each of the sub-processes is used. For instance, between 30-m Landsat 8 and 900-m VLSR LST, the end product is 30-m where 900 pixels of Landsat 8 have acquired the same VLSR LST value in the computation process. We implement these

140 regressions and machine learning approaches again over each study area and at each selected date to ensure the portability of HSR-GEE to other spatial and temporal conditions.

The first used approach concerns the Robust Least Squares (RLS) statistical test. It is used to estimate the unknown parameters in the linear regression model while overcoming several limitations of the standard parametric and non-parametric methods (Davies, 1993). Landsat 8 RGBN bands along the VLSR LST are the independent variables, whereas the

145 Landsat 8 LST is the dependent variable. At the end of the test, five generated coefficients (i.e., over 30-m red, green, blue, near infrared and 900-m LST) along the interception value are generated. The standard equation is as follows:

$$Y = \beta x + \beta'x' + \beta''x'' + etc. + \varepsilon \qquad\qquad Equation\ (1)$$

Where Y is the dependent variable; β, β', β'' are the independent variables; x, x', x'' are the generated weights; and ε is the interception value.

150 We then apply the five generated coefficients along the interception value to 1-m NAIP RGBN and 30-m Landsat LST, respectively. By doing so, we were able to work on the same downscaling ratio (i.e., 30 times) either between 900-m to 30-m and a later stage between 30-m and 1-m, thus enabling the transferability of the generated RLS outputs across different resolutions. This also applies to the other downscaling approaches used in this study.

The second approach used in HSR-GEE is the Random Forests (RF) supervised machine learning algorithm. The number of

155 the used decision trees is 130. RF is a nonparametric "ensemble learning" method trademarked by Leo Breiman and Adele Cutler. It combines the output of multiple decision trees to reach a single result (Chen et al., 2020), handling both classification and regression issues (Breiman, 2001). Its wide adoption is based on his ease of use and flexibility.

Moreover, the Support Vector Machine (SVM) is implemented in this research. It is one of the most popular supervised learning algorithms which was first developed by Vapnik (1995). SVM uses classification algorithms for two-group

160 classification problems, usually for small-and high-dimensional samples (Chang and Lin, 2011).

Over the two RF and SVM machine learning methods, the four Landsat 8 RGBN bands as well as the VLSR LST and the 30-m Landsat 8 LST were used to train RF and SVM classifiers. Later, we apply these generated classifiers over the RGBN bands of NAIP and the 30-m Landsat 8 LST, to compute two 1-m LST images, namely the RF 1-m LST and SVM 1-m LST. For the sake of comparison to other commonly known models, we include both DisTrad and TsHARP in HSR-GEE. DisTrad

165   was first proposed by Kustas et al. (2003). It uses an OLS approach with the NDVI as the independent variable in the equation and was developed over homogenous vegetated areas. TsHARP can be considered as an improvement over DisTrad (Agam et al., 2007), where the more complex FVC is used instead of the NDVI. More information on these two models can be found in Kustas et al. (2003) and Agam et al. (2007).

HSR-GEE system (Figure 2) is freely available on https://bit.ly/3T4HypN, where users can select any time frame and draw

170   or import a study area within CONUS. Six main products will be generated in a matter of seconds, including the original Landsat 8 LST, named L8 LST, a 1-m LST based on RLS, named HSR RLS LST, a 1-m LST based on RF, named HSR RF LST, a 1-m LST based on SVM, named HSR SVM LST, a 1-m LST based on DisTrad, named HSR DisTrad LST and a 1-m LST based on TsHarp, named HSR TsHarp LST.

3 Results

175   ### 3.1 Validations

The validation process resulted in a promising accuracy. Table 2 shows the RMSE and MAE of the HSR LST outputs, namely RLS, RF, SVM DisTrad and TsHARP vis-à-vis the high spatial resolution TIR airborne images in three locations. SVM showed the best accuracy with a RMSE of 1.68°C and a MAE of 1.33°C, followed by RLS with a RMSE of 2.24°C and a MAE of 1.92°C. RF appears to be underperforming with a MAE of 2.53°C but shows an improved accuracy from

180   DisTrad and TsHARP with a MAE of 3.42°C and 3.4°C, respectively. The RMSE frequency distribution histogram in Figures 3 and 4 illustrate the bell-shaped distribution of values over the studied regions, confirming that the random errors in the statistical process for all approaches except for RF can be assumed to be drawn from a Gaussian distribution. While in Hat Creek and Claryville the peak of the distribution is around 0, over the ElKhorn region, high values appear to exist in the category of [-3, -2].

185   ### 3.2 HSR-GEE over ElKhorn, Hat Creek and Claryville

In a visual comparison to Landsat 8 LST, the best detailed downscaling approaches used in HSR-GEE appear to be RLS and RF (Figure 5). Between these two, RF showed LST distributions similar to salt and pepper noise. RLS, on the other hand, was the most conforming to the Landsat 8 LST values. SVM has instead aggregated similar LST values and they can be visually compared to Land Cover/Use maps. For the sake of simplicity and as DisTrad and TsHARP outputs appear to be

190   similar, only TsHARP is included in Figure 5. While over Claryville TsHARP LST appears to be visually identical to the

Landsat 8 LST, it converges in ElKhorn and more in Hat Creek, with most of the LST values appear to be inversed between these two products.

4 Discussion and Conclusion

When validating with the high spatial resolution TIR airborne images, HSR-GEE showed very acceptable accuracy in
195   ElKhorn, Hat Creek and Claryville regions with a MAE below 2.5°C in most cases. This is aligned with other downscaling studies, reporting an error around 3°C, even when using additional bands and indices (e.g., Bonafoni, 2016; Bonafoni et al., 2016; Govil et al., 2019). The lowest MAE was shown using the SVM machine learning approach. As SVM-based outputs showed LST distribution results corresponding to the Land Cover/Use maps, the integration of the Local Climate Zone (LCZ), as it was suggested in previous studies particularly over urban regions (e.g., Bechtel et al., 2012; Xia et al., 2022),
200   might better represent the LST distribution at a 1-m scale. In contrast to previous studies (e.g., Liu et al., 2017; Talukdar et al., 2020) that were conducted at different spatial scales, RF had least performed at the 1-m spatial scale with a noticeable salt and pepper effect. When the most commonly used standard DisTrad and TsHARP downscaling models were applied, the MAE of ~3.42°C appears to be larger than the three used approaches (e.g., RLS, RF and SVM) and worse visually. DisTrad and TsHARP biases appear to be aligned with the number of considered pixels in the study area (i.e., MAE of ~1, ~2.6 an
205   ~6.6 in areas of ~70 000, ~900 000 and ~1 300 000 pixels, respectively). As a result, these two models appear to be not designed for large and heterogeneous areas. RLS remains then the most adequate downscaling approach at the 1-m spatial scale, providing detailed LST layers and at a promising accuracy. Anyhow, the bell-shaped curves of the RMSE frequency distribution histograms for RLS and SVM assume that the observed random errors are drawn from a normal distribution, and Therefore, HSR-GEE can be accurately implemented over the CONUS.

210   It is important to note that the peak shift found in the RLS RMSE frequency distribution histogram can be related to the usage of a Landsat 8 image a month prior to the TIR image (i.e., December 15th, 2017 for TIR vs. November 11th, 2017 for Landsat 8) due to unavailability of images with a shorter time gap. What was interesting though is that both RF and SVM have automatically accounted for this difference and their RMSE frequency distribution histograms are centred around 0.

Few limitations appear in HSR-GEE. The most prominent would be the usage of the three-year NAIP images, where
215   monthly variations could not be fully captured. In this context, it is not advised to use HSR-GEE for crop assessment at different development stages or in the case of volcanic emissions, even though the system includes an internal calibration process (i.e., bandpass adjustment) to convert NAIP bands into real time Landsat 8 bands. Another limitation is the restriction of HSR-GEE over CONUS only, as NAIP is only available over that region. Still, future studies can attempt to implement HSR-GEE over multiple regions across the Globe when offline or cloud-based HSR images are available.

220   Anyhow, the proposed HSR-GEE sets a novel direction in LST downscaling based on HSR RGBN images only. This system is simple, easy-to-use, freely-available, and automatically implementing five different downscaling approaches over the GEE platform. The HSR-GEE system is much needed as the LST parameter is considered in many studies and applications related

to the environment, agriculture, and cities. To our knowledge, the HSR-GEE system is the first to downscale LST values to a 1-m spatial resolution, using only RGBN bands from HSR images. Furthermore, the usage of a minimal number of bands is
225 a great asset since commercial HSR images come with a limited number of bands and in some cases the addition of bands to images would increase the cost of these images extravagantly. This algorithm will benefit researchers from different disciplines to conduct further applications and analysis at the city block and neighbourhood scales, but also to improve the understanding of LST value distribution at the 1-m scale.

5 Computer code availability

230 Name: HSR-GEE

Developer: Mario Mhawej, Yaser Abunnasr

E-mail: mm278@aub.edu.lb

Year first available: 2022

hardware required: GPU

235 software required: none

program language: JavaScript

Source code: *https://bit.ly/3T4HypN; https://code.earthengine.google.com/e5dd5f5f5265028e136928f10d07b114*

6   Author contribution

Yaser Abunnasr: Conceptualization, Methodology, Analysis, Writing. Mario Mhawej: Conceptualization, Methodology,
240 Data acquisition, Implementation, Analysis, Writing.

References

1. Agam, Nurit, William P. Kustas, Martha C. Anderson, Fuqin Li, and Christopher MU Neale. "A vegetation index based technique for spatial sharpening of thermal imagery." Remote Sensing of Environment 107, no. 4 (2007): 545-558.

2. Allam, Mona, Mario Mhawej, Qingyan Meng, Ghaleb Faour, Yaser Abunnasr, Ali Fadel, and Hu Xinli. "Monthly 10-m
245 evapotranspiration rates retrieved by SEBALI with Sentinel-2 and MODIS LST data." Agricultural Water Management 243 (2021): 106432.

3. Allaw, Kamel, Hamze Ali, Faour Ghaleb, Mhawej Mario, and Ghossain Tony. "GIS-based mapping of areas sensitive to desertification in a semi-arid region in Lebanon." South-Eastern European Journal of Earth Observation and Geomatics 4 (2015): 91-103.

250   4.   Abunnasr, Yaser, Mario Mhawej, and Nektarios Chrysoulakis. "SEBU: A novel fully automated Google Earth Engine surface energy balance model for urban areas." Urban Climate 44 (2022): 101187.

5.   Bechtel, Benjamin, Klemen Zakšek, and Gholamali Hoshyaripour. "Downscaling land surface temperature in an urban area: A case study for Hamburg, Germany." Remote Sensing 4, no. 10 (2012): 3184-3200.

6.   Bechtel, Benjamin, Klemen Zakšek, and Gholamali Hoshyaripour. "Downscaling land surface temperature in an urban
255   area: A case study for Hamburg, Germany." Remote Sensing 4, no. 10 (2012): 3184-3200.

7.   Bonafoni, Stefania, Roberta Anniballe, Beniamino Gioli, and Piero Toscano. "Downscaling Landsat land surface temperature over the urban area of Florence." European Journal of Remote Sensing 49, no. 1 (2016): 553-569.

8.   Bonafoni, Stefania. "Downscaling of Landsat and MODIS land surface temperature over the heterogeneous urban area of Milan." IEEE Journal of Selected Topics in Applied Earth Observations and Remote Sensing 9, no. 5 (2016): 2019-
260   2027.

9.   Breiman, Leo. "Random Forests. Statistics Department." University of California, Berkeley, CA 4720 (2001).

10.   Briggs, M.A., Dawson, C.B., White, E.A., Gazoorian, C.L., Hare, D.K., and Lane, J.W., 2020, Thermal infrared and photogrammetric data collected by drone for hydrogeologic characterization around two US Geological Survey Next Generation Water Observing Systems stream gage locations near Claryville, NY, USA: U.S. Geological Survey data
265   release, https://doi.org/10.5066/P9FIZTPU.

11.   Chang, Chih-Chung, and Chih-Jen Lin. "LIBSVM: a library for support vector machines. http." www, csie. ntu. edu. tw/-cjlin/libsvm (2001).

12.   Chen, Cheng, Qiuwen Chen, Binni Qin, Shuhe Zhao, and Zheng Duan. "Comparison of different methods for spatial downscaling of GPM IMERG V06B satellite precipitation product over a typical arid to semi-arid area." Frontiers in
270   Earth Science (2020): 525.

13.   Cho, Kangjoon, Yonghyun Kim, and Yongil Kim. "Disaggregation of Landsat-8 thermal data using guided SWIR imagery on the scene of a wildfire." Remote Sensing 10, no. 1 (2018): 105.

14.   Claverie, Martin, Junchang Ju, Jeffrey G. Masek, Jennifer L. Dungan, Eric F. Vermote, Jean-Claude Roger, Sergii V. Skakun, and Christopher Justice. "The Harmonized Landsat and Sentinel-2 surface reflectance data set." Remote sensing
275   of environment 219 (2018): 145-161.

15.   Curtis, J.A., Torgersen, C.E., Diabat, M., Mejia, F.H., Marcelli, M.F., Burns, E.R., Wheelock, S.J., and Slotke, A., 2021, Airborne thermal infrared imagery and longitudinal stream temperature profiles, Hat Creek, California, August 2018: U.S. Geological Survey data release, https://doi.org/10.5066/P9DMJYT7.

16.   Davies, Patrick L. "Aspects of robust linear regression." The Annals of statistics (1993): 1843-1899.

280   17.   Demuzere, Matthias, K. Orru, O. Heidrich, El Olazabal, D. Geneletti, Hans Orru, A. G. Bhave, N. Mittal, E. Feliu, and Maija Faehnle. "Mitigating and adapting to climate change: Multi-functional and multi-scale assessment of green urban infrastructure." Journal of environmental management 146 (2014): 107-115.

18. Dialesandro JM, SM Wheeler, Y Abunnasr. "Urban heat island behaviors in dryland regions." Environmental Research Communications 1 (8), 081005

19. Dozier, Jeff. "A method for satellite identification of surface temperature fields of subpixel resolution." Remote Sensing of environment 11 (1981): 221-229.

20. Essa, Wiesam, Johannes van der Kwast, Boud Verbeiren, and Okke Batelaan. "Downscaling of thermal images over urban areas using the land surface temperature–impervious percentage relationship." International Journal of Applied Earth Observation and Geoinformation 23 (2013): 95-108.

21. Faour, Ghaleb, and Mario Mhawej. "Mapping urban transitions in the Greater Beirut area using different space platforms." Land 3, no. 3 (2014): 941-956.

22. Faour, Ghaleb, Mario Mhawej, and Abbas Fayad. "Detecting Changes in Vegetation Trends in the Middle East and North Africa (MENA) Region Using SPOT Vegetation." Cybergeo: European Journal of Geography (2016).

23. Faour, Ghaleb, Mhawej Mario, and Abou Najem Sandra. "Regional landsat-based drought monitoring from 1982 to 2014." Climate 3, no. 3 (2015): 563-577.

24. Gao, Feng, William P. Kustas, and Martha C. Anderson. "A data mining approach for sharpening thermal satellite imagery over land." Remote Sensing 4, no. 11 (2012): 3287-3319.

25. Giglio, Louis, Jacques Descloitres, Christopher O. Justice, and Yoram J. Kaufman. "An enhanced contextual fire detection algorithm for MODIS." Remote sensing of environment 87, no. 2-3 (2003): 273-282.

26. Gorelick, Noel, Matt Hancher, Mike Dixon, Simon Ilyushchenko, David Thau, and Rebecca Moore. "Google Earth Engine: Planetary-scale geospatial analysis for everyone." Remote sensing of Environment 202 (2017): 18-27.

27. Govil, Himanshu, Subhanil Guha, Anindita Dey, and Neetu Gill. "Seasonal evaluation of downscaled land surface temperature: A case study in a humid tropical city." Heliyon 5, no. 6 (2019): e01923.

28. Guillevic, P., F. Göttsche, J. Nickeson, G. Hulley, D. Ghent, Y. Yu, I. Trigo et al. "Land surface temperature product validation best practice protocol. Version 1.1." Best Practice for Satellite-Derived Land Product Validation 60 (2018).

29. Hobza, C.M., and Strauch, K.R., 2019, Water-level and aerial thermal infrared imagery data collected along the lower Platte and Elkhorn Rivers, Nebraska, 2016-2017: U.S. Geological Survey data release, https://doi.org/10.5066/P9EZLGSC.

30. Hutengs, Christopher, and Michael Vohland. "Downscaling land surface temperatures at regional scales with random forest regression." Remote Sensing of Environment 178 (2016): 127-141.

31. Hutengs, Christopher, and Michael Vohland. "Downscaling land surface temperatures at regional scales with random forest regression." Remote Sensing of Environment 178 (2016): 127-141.

32. Kustas, William P., John M. Norman, Martha C. Anderson, and Andrew N. French. "Estimating subpixel surface temperatures and energy fluxes from the vegetation index–radiometric temperature relationship." Remote sensing of Environment 85, no. 4 (2003): 429-440.

33. Liu, Desheng, and Ruiliang Pu. "Downscaling thermal infrared radiance for subpixel land surface temperature retrieval." Sensors 8, no. 4 (2008): 2695-2706.

34. Liu, Yangxiaoyue, Yaping Yang, Wenlong Jing, and Xiafang Yue. "Comparison of different machine learning approaches for monthly satellite-based soil moisture downscaling over Northeast China." Remote Sensing 10, no. 1 (2017): 31.

35. Maiti, Somnath, Rajat Satpathy, Jatisankar Bandyopadhyay, and A. T. Jeyaseelan. "Vegetation Parameter Derivation for Forest Health Measurement and Stress Detection in a Time Series." Research & Reviews: Journal of Ecology 4, no. 3 (2018): 19-26.

36. Mhawej, Mario, Ali Fadel, and Ghaleb Faour. "Evaporation rates in a vital lake: a 34-year assessment for the Karaoun Lake." International Journal of Remote Sensing 41, no. 14 (2020c): 5321-5337.

37. Mhawej, Mario, Arnaud Caiserman, Ali Nasrallah, Ali Dawi, Roula Bachour, and Ghaleb Faour. "Automated evapotranspiration retrieval model with missing soil-related datasets: The proposal of SEBALI." Agricultural Water Management 229 (2020a): 105938.

38. Mhawej, Mario, Georgie Elias, Ali Nasrallah, and Ghaleb Faour. "Dynamic calibration for better SEBALI ET estimations: Validations and recommendations." Agricultural Water Management 230 (2020b): 105955.

39. Mhawej, Mario, Ghaleb Faour, Abbas Fayad, and Amin Shaban. "Towards an enhanced method to map snow cover areas and derive snow-water equivalent in Lebanon." Journal of Hydrology 513 (2014): 274-282.

40. Mhawej, Mario, Ghaleb Faour, Chadi Abdallah, and Jocelyne Adjizian-Gerard. "Towards an establishment of a wildfire risk system in a Mediterranean country." Ecological informatics 32 (2016): 167-184.

41. Pan, Xin, Xi Zhu, Yingbao Yang, Chen Cao, Xize Zhang, and Liangliang Shan. "Applicability of downscaling land surface temperature by using normalized difference sand index." Scientific reports 8, no. 1 (2018): 1-14.

42. Pu, Ruiliang, and Stefania Bonafoni. "Reducing Scaling Effect on Downscaled Land Surface Temperature Maps in Heterogenous Urban Environments." Remote Sensing 13, no. 24 (2021): 5044.

43. Stathopoulou, Marina, and Constantinos Cartalis. "Downscaling AVHRR land surface temperatures for improved surface urban heat island intensity estimation." Remote Sensing of Environment 113, no. 12 (2009): 2592-2605.

44. Talukdar, Swapan, Pankaj Singha, Susanta Mahato, Swades Pal, Yuei-An Liou, and Atiqur Rahman. "Land-use land-cover classification by machine learning classifiers for satellite observations—A review." Remote Sensing 12, no. 7 (2020): 1135.

45. Vapnik Vladimir, N. "The nature of statistical learning theory." (1995).

46. Wang, Liming, Fuqiang Tian, Xufeng Wang, Yanzheng Yang, and Zhongwang Wei. "Attribution of the land surface temperature response to land-use conversions from bare land." Global and Planetary Change (2020): 103268.

47. Xia, Haiping, Yunhao Chen, Conghe Song, Junxiang Li, Jinling Quan, and Guomo Zhou. "Analysis of surface urban heat islands based on local climate zones via spatiotemporally enhanced land surface temperature." Remote Sensing of Environment 273 (2022): 112972.

350   48. Xu, Nuo, Fan Deng, Bingqi Liu, Caixia Li, Hancong Fu, Huan Yang, and Jiahua Zhang. "Changes in the urban surface thermal environment of a Chinese coastal city revealed by downscaling MODIS LST with random forest algorithm." Journal of Meteorological Research 35, no. 5 (2021): 759-774.

49. Yang, Yingbao, Chen Cao, Xin Pan, Xiaolong Li, and Xi Zhu. "Downscaling land surface temperature in an arid area by using multiple remote sensing indices with random forest regression." Remote Sensing 9, no. 8 (2017): 789.

355   50. Zakšek, Klemen, and Krištof Oštir. "Downscaling land surface temperature for urban heat island diurnal cycle analysis." Remote Sensing of Environment 117 (2012): 114-124.

51. Zakšek, Klemen, and Krištof Oštir. "Downscaling land surface temperature for urban heat island diurnal cycle analysis." Remote Sensing of Environment 117 (2012): 114-124.

52. Zhan, Wenfeng, Yunhao Chen, Ji Zhou, Jinfei Wang, Wenyu Liu, James Voogt, Xiaolin Zhu, Jinling Quan, and Jing Li.
360   "Disaggregation of remotely sensed land surface temperature: Literature survey, taxonomy, issues, and caveats." Remote Sensing of Environment 131 (2013): 119-139.
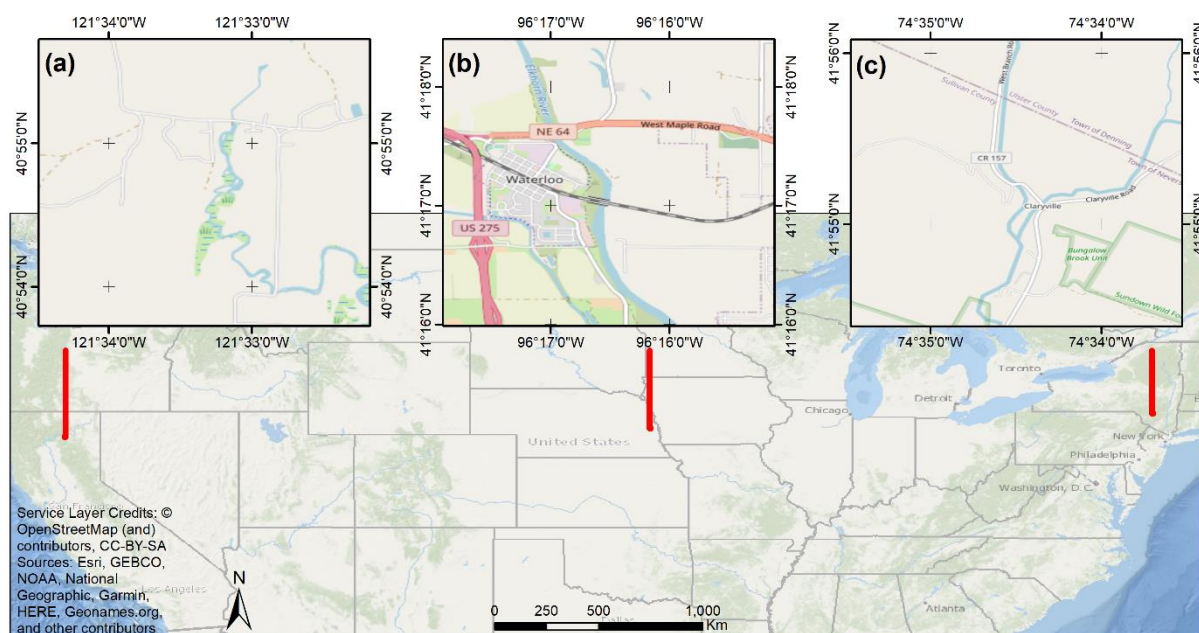
Figure 1: Location of the studied regions, including from left to right, (a) Hat Creek, (b) ElKhorn and (c) Claryville.

365

Figure 2: A snapshot of the HSR-GEE system showing the 1-m RLS LST product.
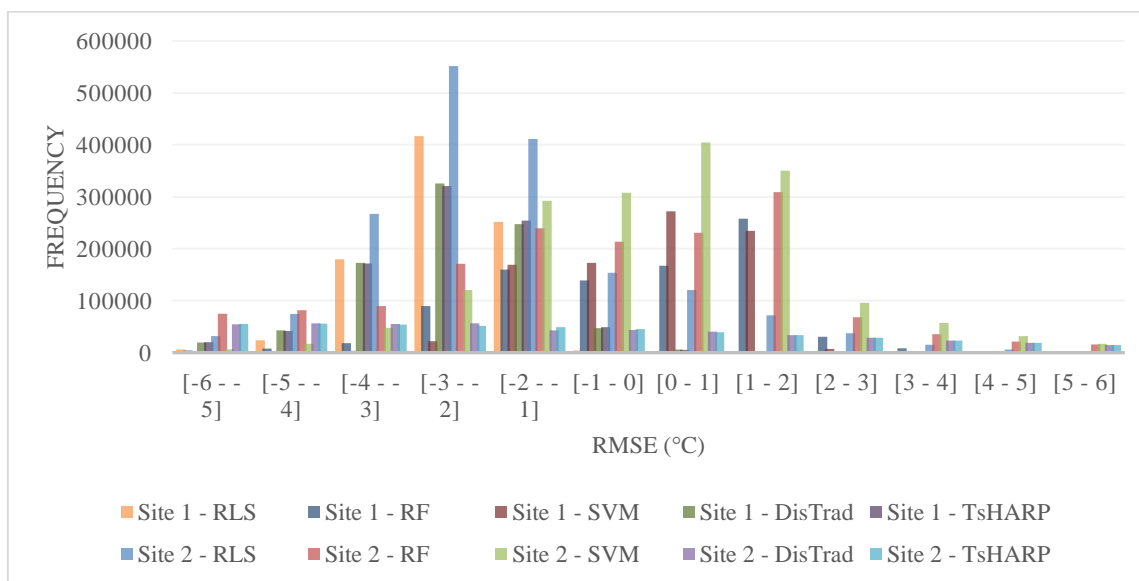
370   **Figure 3: A RMSE frequency distribution histogram showing the relationship between the 1-m LST products (i.e., RLS, RF, SVM, DisTrad and TsHARP) and the respective thermal images after applying the dT factor over the two study regions (Site 1: ElKhorn; Site 2: Hat Creek; n≈2 200 000).**
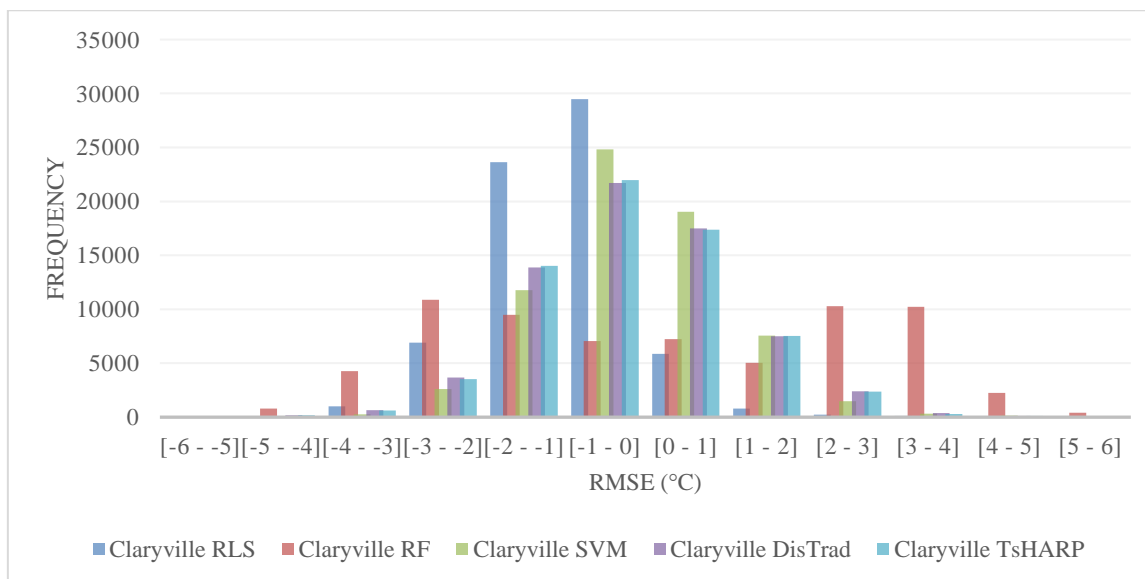
Figure 4: A RSME frequency distribution histogram showing the relationship between the 1-m LST products (i.e., RLS, RF, SVM, DisTrad and TsHARP) and the respective thermal images after applying the dT factor over Claryville (n≈70 000).
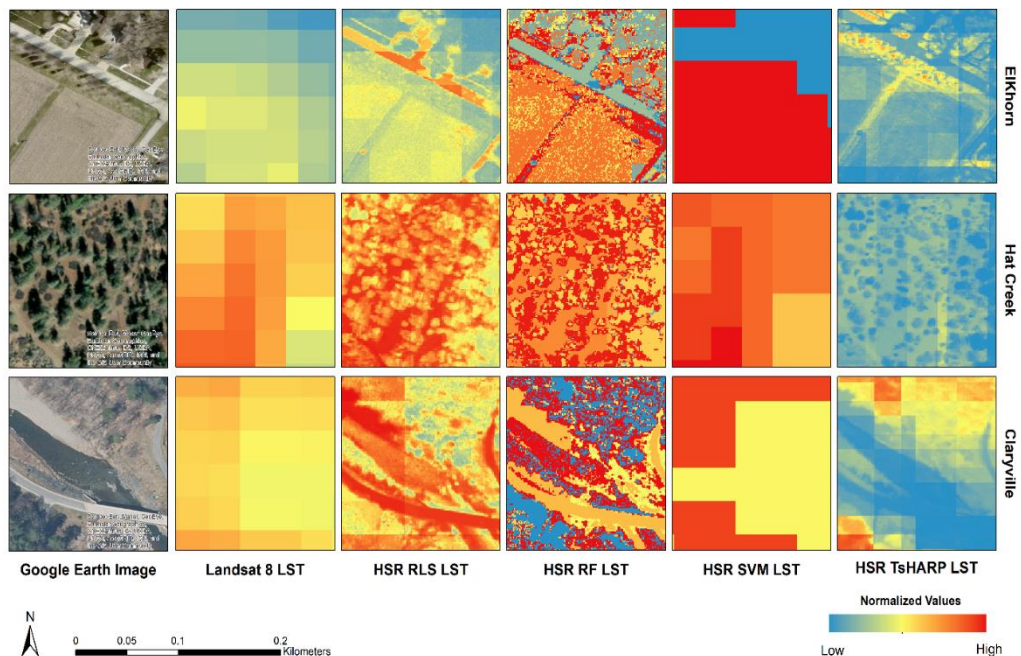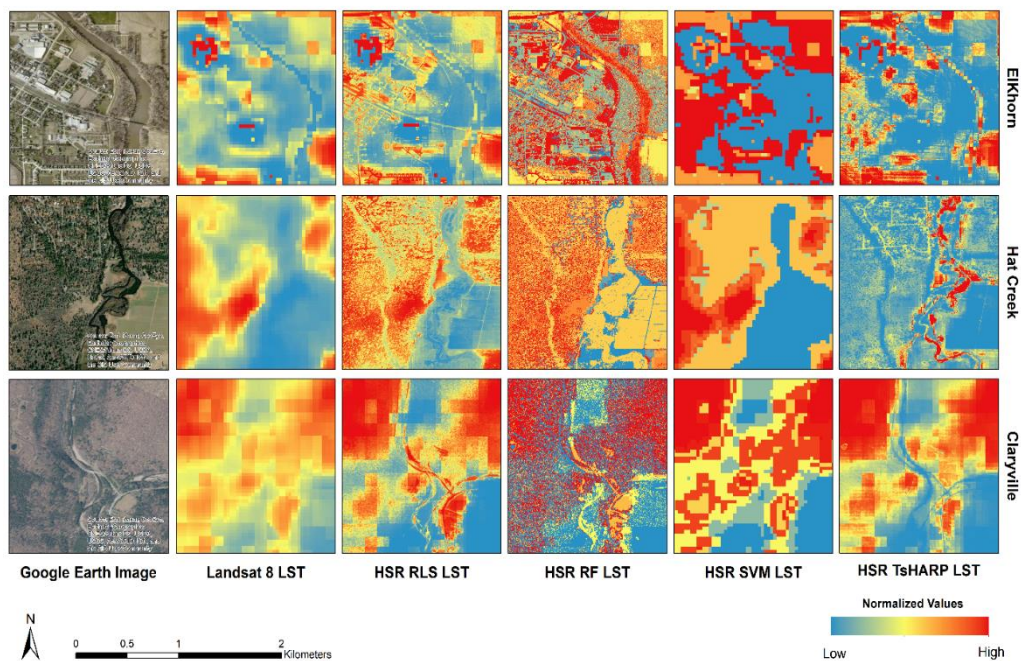
Figure 5: A comparison between Landsat 8 LST and HSR-GEE outputs (i.e., RLS, RF, SVM and TsHARP LSTs) over ElKhorn, Hat Creek and Claryville on 1:20 000 (top) and 1:2 000 (bottom) scales (Satellite images source from © Google Earth)

380

Table 1: Airborne TIR and Landsat 8 satellite images overpass time used for validations over ElKhorn, Hat Creek and Claryville.

Location	TIR overpass time	Landsat 8 overpass time
ElKhorn	December 15th, 2017	November 11th, 2017
Hat Creek	August 25th, 2018	August 27th, 2018
Claryville	December 8th and 10th, 2019	October 11th, 2019

385 **Table 2: RMSE and MAE between the 1-m LST products (i.e., RLS, RF, SVM, DisTrad and TsHARP) and the respective thermal images after applying the dT factor over the three study regions.**

Site	Date	Sample Size	RLS RMSE (°C)	RLS MAE (°C)	RF RMSE (°C)	RF MAE (°C)	SVM RMSE (°C)	SVM MAE (°C)	DisTrad MAE (°C)	TsHARP MAE (°C)
ElKhorn	12/15/2017	~900 000	2.65	2.53	1.71	1.41	1.26	1.04	2.62	2.6
Hat Creek	8/25/2018	~1 300 000	2.74	2.12	4.82	3.99	2.64	2.06	6.64	6.59
Claryville	10/10/2019	~70 000	1.33	1.1	2.49	2.18	1.15	0.89	1.02	1.01
Average			**2.24**	**1.92**	**3.01**	**2.53**	**1.68**	**1.33**	**3.42**	**3.4**